18th Australasian Fluid Mechanics Conference
Launceston, Australia
3-7 December 2012

Numerical and *in vitro* experimental study of arterial deformation and buckling under hypertension and atherosclerotic conditions

P. Assemat[1], G. Hannema[1], J. Carberry[1], D. Michell[2], K. Andrews[2], A. Dart[2],J. Chin-Dusting[2] and K. Hourigan[1]

[1] Department of Mechanical and Aerospace Engineering and Division of Biological Engineering
Monash University, Victoria 3800, Australia

[2] Baker IDI Heart and Diabetes Institute
75 Commercial Rd, Melbourne, Victoria 3004, Australia

Abstract

Cardiovascular diseases remain the major cause of mortality worldwide. Pathologies of the vasculature such as atherosclerosis are often related to biochemical and genetic factors as well as mechanical effects that strongly change the function and shape of arteries. The present work is part of a general research project which aims to better understand the mechanical mechanisms responsible for atherosclerotic plaque formation and rupture. The chosen approach is to use numerical fluid structure interaction (FSI) methods to study the relative influence of hemodynamic parameters on the structural stresses generated on plaques. To this aim, a numerical study of a simplified straight vessel exposed to lumen pressure was investigated under quiescent and steady flow conditions. As the internal pressure or the steady velocity increases, the vessel buckles leading to a non-linear large deformation behaviour. The results have been validated using theoretical predictions for the buckling thresholds. Further studies on idealised cardiovascular conditions such as stenosis (i.e., lumen constriction) or aneurysm like (i.e., arterial wall expansion) formation have also been performed.

Introduction

Atherosclerosis occurs due to the build-up and infiltration of lipid streaks in artery walls, leading to plaques. It is an inflammatory disease characterized by a succession of biochemical and biomechanical complex processes [3, 12]. In plaques, the lipid core is separated from the circulating blood by a fibrous cap of variable thickness. As plaques develop, they induce a remodelling of the arteries [15]. Plaques can be divided into two distinct types: those that rupture (vulnerable) and those that are less likely to rupture (stable), a characteristic that is associated in some papers to the respective aneurysm-like and stenotic shapes [5]. While it is accepted that plaque vulnerability is influenced by fibrous cap thickness and the size of the lipid core [1], it also depends on artery remodelling, the loads applied on the solid and the forces induced by the fluid for which no general agreement has been found.

The complexity of the present problem comes from the coupling of biological, chemical and mechanical effects. In the following, the literature review will be restricted to the influence of mechanical effects on plaque rupture. Most of the numerical studies in real arteries performed until now focus on the calculation of the flow around plaques, considering the arteries as rigid walls [2, 6]. These papers indicate that the high wall shear stress (WSS) found on plaques could be responsible for plaque rupture; however, Sadat et al. [13] showed recently that structural stresses are thought to play a more important role, being several orders of magnitude higher than the WSS induced by blood flow. To calculate the structural stresses, a complex FSI approach taking into account large deformations is required. A three-dimensional (3D) fluid structure interaction model has revealed an association between regions of high plaque critical stress and fibrous cap disruption in human carotid [16]. Furthermore, maximum principal stresses were identified on shoulder regions of the fibrous caps of carotid plaques according to 2D FSI simulations [9]. An histology based finite element analysis was used to investigate the peak circumferential stresses in aortic and brachiocephalic plaques of ApoE -/- mice [19]. Their results showed the aortic plaque stresses only slightly depend on the cap thickness whereas for the brachiocephalic artery lesions, it is shown that there is an exponential growth of peak cap stress with decreasing cap thickness. Altogether, these recent papers underline the multiplicity of the origins of plaque rupture and the complexity of finding a general agreement of the main parameters that engender this event. In addition, very few computational studies have considered the elastic properties of arteries or have investigated the hemodynamic parameters and mechanical forces induced in realistic vessel geometry by a blood flow past plaque. Therefore, developing simplified FSI models under those requirements is a starting point towards further understanding of atherosclerotic development.

The complexity of the task comes from the large number of influential parameters involved in the mechanical model (geometrical parameters, transmural pressure (external internal pressure), oscillating flow rate, variable elasticity and density properties of the tissues, non-Newtonian effects). In the present work, the geometries considered are restricted to straight vessels and straight vessels with stenosis (stable shape). In addition to the physical parameters, a large number of numerical parameters must be checked in order to insure the convergence of the numerical methods as large deformations are involved. Indeed, in the physiological range of parameters, it has been shown [7] that straight vessels buckle when a critical transmural pressure is reached. In addition, whilst the general dynamics of fluid-conveying systems have been already studied for “rigid” materials [11], in the present study, materials with weak Young’s modulus are considered, as well as the coupling of flow and high transmural pressure, effects which together have implications on the mechanical stability of the system. Hence, within physiological range, vessels are readily prone to large deformation.

In the following, after the presentation of the model, the numerical approach will be described and compared to linear theory. In addition, a description of the method used to extract the elastic properties from the experiments will be presented. Some key results will be presented at the end of the article.

Model

Geometry

The model used in the present study follows the work of Young and Tsai [21] who developed an axisymmetric model to represent the stenosis:

$$r(z) = \frac{D}{2} - \frac{\delta_s}{2}\left[1+\cos\left(\frac{\pi z}{Z_s}\right)\right], \quad (1)$$

where $r(z)$ represents the radius of the vessel, D_s the stenosis diameter at the maximum constriction location ($z=0$), Z_s half of the stenosis length and δ_s the stenosis height $\delta_s = (D-D_s)/2$. This geometry is represented figure 1. Most of the paper will concern straight vessel for which $\delta_s = 0$.

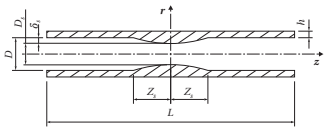

Figure 1: Model geometry of an idealised axisymmetric stenotic vessel.

Model equations

The fluid and solid behaviour are described by the following coupled equations:

$$\rho_f\left(\frac{\partial \mathbf{U}}{\partial t} + (\mathbf{U}\cdot\nabla)\mathbf{U}\right) = \nabla\cdot\bar{\bar{\sigma}}_f, \quad (2)$$

$$\nabla\cdot\mathbf{U} = 0, \quad (3)$$

$$\rho_s\left(D_{tt}\eta - \mathbf{f_s}\right) = \nabla\cdot\bar{\bar{\sigma}}_s, \quad (4)$$

where ρ_f is the fluid density, $\mathbf{U}$ the 3D velocity field and $\bar{\bar{\sigma}}_f$ the fluid stress tensor:

$$\bar{\bar{\sigma}}_f = -P\bar{\bar{I}} + \mu\left(\nabla\mathbf{U} + \nabla\mathbf{U}^T\right), \quad (5)$$

with $\bar{\bar{I}}$ the unit tensor, P the pressure and μ the dynamic viscosity of the fluid. In the solid equation, ρ_s represents the material density, D_t the material derivative, η the 3D structure displacement, $\mathbf{f_s}$ the body force and $\bar{\bar{\sigma}}_s$ the structural stress tensor. Concerning the boundary conditions: a Poiseuille velocity profile is imposed at the inlet when flow is considered whereas $\partial P/\partial z = 0$ at the outlet. At the fluid solid interface, the boundary conditions are:

$$\bar{\bar{\sigma}}_f\cdot\mathbf{n}_f = -\bar{\bar{\sigma}}_s\cdot\mathbf{n}_s, \quad (6)$$

$$\mathbf{U} = \partial_t\eta. \quad (7)$$

In addition, a contant atmospheric pressure is applied along the external surface of the solid. The remaining term to be determined is $\bar{\bar{\sigma}}_s$ which depends on the material properties of the solid and on the strain (ε). The calculation of this term will be detailed in the next section. For the numerical calculation, the dynamic viscosity, fluid and solid densities remain constant with $\mu = 4.10^{-3} Pa.s$ [18], $\rho_f = \rho_s = 1060 kg/m^3$ [4]. As a consequence, the fluid is considered Newtonian, a reasonable assumption provided the shear rate is greater than $150 s^{-1}$ [20], which is the case in the range of parameters considered for the present study. The density of the solid has been considered equal to the fluid in order to prevent the influence of the gravity effects. This approximation is acceptable considering that in a recent study [14], Shinohara et al. showed that the density parameter range for the plaque and the artery walls is $1010 - 1080 kg/m^3$.

Stuctural stress tensor and theoretical divergence model

Structural stress tensor

The arterial walls are hyperelastic material for which the elasticity properties, the Young's modulus, depends non-linearly on the load applied on the vessel; however, in the present study, only orthotropic (linear) material will be considered in order to validate our FSI model. The method described in the following indicates how to extract the constant axial and circumferencial Young's modulus from experiments.

Following the work of Liu and Han [10], free inflation test has been performed. The method consists of imposing an internal pressure, the vessel being plugged at one extremity (figure 2). The expansion of the vessel in the axial and longitudinal directions is recorded by a camera on the top. The pressure is increased to measure its influence on the deformation of the vessel (stretch). From the obtained stretch versus pressure curves, the structural stresses σ_s can be calculated using Lame's equations. As the Young's modulus E is a function of the strain ε, the relation between stress and strain is $\sigma_s = E(\varepsilon)\varepsilon$. Figure 3 indicates the stress as a function of the strain for a rat carotid. A constant Young's modulus is then extracted by calculating the slope of the lines indicated on figure 3. Thoses lines are obtained by imposing the following equality using energy arguments.

$$\int_0^{\varepsilon_p}\sigma_s d\varepsilon = \bar{E}(\varepsilon_p)\left[\frac{1}{2}\varepsilon^2\right]_0^{\varepsilon_p}, \quad (8)$$

where ε_p is chosen accordingto a pressure of interest.

Figure 2: View of the experimental inflation test in rat carotid.

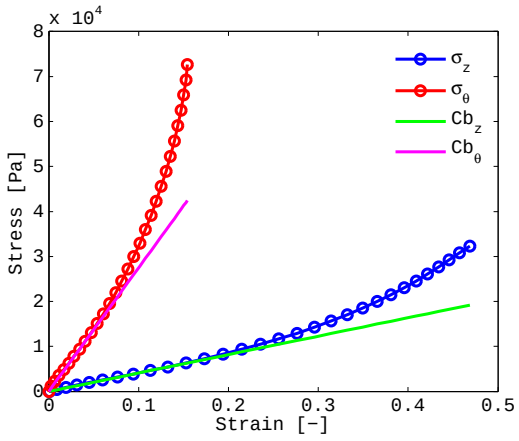

Figure 3: Stress-strain relation obtained from the stretch-pressure curves in [10] using the method described in the present section. The blue curve corresponds to axial stress and the red curve to the circumferencial stress. The lines correpond to the linear approximation defined equation 8.

Further information on the procedure can be found in [8]. The other parameter, the Poisson ratio, necessary to describe the elastic properties of the tissue, is fixed to $\nu = 0.49$ (nearly incompressible material).

Theoretical buckling model

To validate the numerical results, a comparison with the theory has been performed. In [11], the author indicates that the dynamics of buckling of cylindrical structures can be modeled in first approximation by the following one dimensional equation:

$$EI\frac{\partial^4 w}{\partial x^4} + \left\{MU^2 - \bar{T} + \bar{p}A(1-2\nu\delta)\right\}\frac{\partial^2 w}{\partial x^2} + 2MU\frac{\partial^2 w}{\partial x \partial t} + (M+m)\frac{\partial^2 w}{\partial t^2} = 0, \quad (9)$$

where E corresponds to the Young's modulus in the axial direction (E_z), I to the area moment of inertia, w to the lateral deflection, $\bar{T}$ to the externally applied tensions, $\bar{p}$ to the mean pressure, ν to the Poisson ratio and δ depends on boundary condition (in our case, closed pressure vessel $\delta = 0$). In addition, M is the mass of the fluid flow per unit length and m the mass of the pipe per unit length.

As divergence is a static rather than a dynamic form of instability, one needs to consider only the time-independent terms of equation [11] to analyse the dynamics of the system. Hence, the critical buckling pressure can be obtained following a procedure similar to [17] and is given by:

$$\bar{p}_{critical} = \frac{4}{\pi D^2}\left[\frac{4\pi^2 EI}{L_k^2} + \bar{T} - MU^2\right], \quad (10)$$

where L_k represents the buckling length, which depends on the length of the vessel, and on the boundary conditions (in the present case $L_k = L/2$).

Numerical approach and validation

The software codes used to solve the equation are Ansys CFX for the fluid and Ansys Mechanical APDL for the structure. ANSYS CFX is an element-based finite-volume method with second-order accurate discretization schemes in space and time. Ansys Mechanical APDL uses a finite element based structural solver. In this study, hexahedral quadratic elements are used for the spatial discretisation of both fluid and solid domains. The coupling between the fluid and the structural solver is achieved using Ansys Multi-field solver capabilities for which field variables (displacement and forces) are exchanged between both solvers through the fluid-structure interface in an iterative process. For the mesh, attention has been paid to define the characteristic size of the grid cells in the fluid near the interface. This size must be compatible with the capture of the boundary layer (the first computational cell is located within the viscous sublayer) but it must prevent the folding of the mesh due to large deformations(large cells). A compromise has been found to fulfill these two requirements (figure 4) and to optimize the radial mesh distribution. The method used to define the mesh in the fluid part is an O-grid method.

A numerical parameter sensitivity study, not presented here, has been performed on the vessel studied by [10]. For $L = 45mm$, $D = 3.38mm$ and $h = 1mm$, the optimal mesh distribution is 36 nodes in the circumferential direction and 100 in the axial one. The time step is 0.005s. The pressure is increased linearly in time to reach 100mmHg (physiological pressure). The Young's modulus calculated from [10] and used for the present calculation are $E_z = 45.5KPa$ and $E_r = 308.6KPa$. The code has been validated comparing the buckling critical pressure in straight vessels to the theory by setting $U = \bar{T} = 0$ in equation 10. The numerical buckling critical pressure is defined as the transition between the axisymetric expansion and the sinusoidal shape observation. The mean variation between theoretical prediction and numerical approach is around 5% when the length and the thickness of the vessels are varied. The post buckling behaviour will be discussed in the next section.

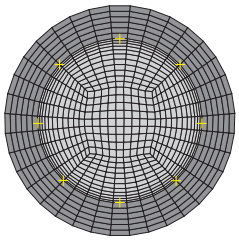

Figure 4: Typical mesh slice representing the fluid domain (inner disk - light grey filling) and the solid domain (outer disk - dark grey filling).The monitor points represented by crosses are used to track the system evolution.

Results

In this paragraph, few results will be presented and discussed. Figure 5 shows a comparison between experimental and numerical results for an internal pressure of 95mmHg (post-buckling regime). A good qualitative agreement is obtained between the experimental and numerical approach, the deformation being of the same order as the internal pressure increased from 0 to 95 mmHg. Additional improvements are needed to obtain a quantitative matching, including taking into account the hyper-elastic properties of the vessel wall. A steady flow state with a flow

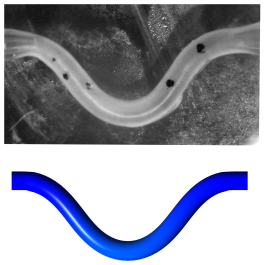

Figure 5: Comparison between experimental (upper frame) and numerical (lower frame) buckled mode shape at a lumen pressure of 95mmHg.

rate of $160ml/min$ [10] has been added to the previous configuration. Its destabilising effect induces a reduction in the critical buckling pressure. Again, the results have been compared to the linear theory and an acceptable mean error of 6% has been obtained. For the model vessel whose dimensions have been described in the previous section, the numerical critical pressure is 24.8mmHg compared to 25.303 in theory.

Finally, numerical simulations were conducted on stenotic and aneurysm-like vessels. Results are only presented here for a stenotic configuration. Figure 6 shows the Von Mises stresses for a vessel with 60% stenosis (percentage of fluid domain narrowing) for an internal pressure of 60mmHg. The maximal stress on the plaque is located along the fluid solid interface (the fibrous cap), location at which the stenosis is the most stretched and compressed by the buckling phenomenon. A close examination of figure reveals that local maxima are observed on the inner side of the buckling at the shoulder of the stenosis (boundary between the stenosis and the healthy wall), a result compatible with the 2D simulation of [9]. In addition, it has been found that the maximum of the structural stress increases when the pressure increases (not presented here [8]), a result in agree-

ment with the fact that people with hypertension (higher internal pressure) suffer more cardivascular conditions.

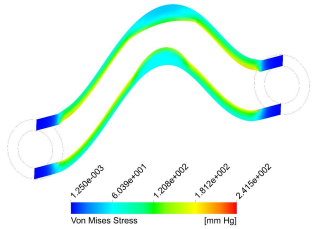

Figure 6: Von Mises stresses in a buckled axisymmetric stenosis at 60$mmHg$.

Conclusion and discussion

An FSI model has been developed for simplified axisymmetric geometries. Characteristic vessel dimensions found in the literature [10] as well as experimental samples of rat carotid aortas were used to calculate realistic Young's modulus and to validate an FSI approach. The FSI model was able to predict the buckling threshold within a range of physiological parameters under both quiescent and steady state flow. Furthermore idealised cardiovascular conditions were modelled by axisymmetric stenosis. The stability analysis permitted to highlight zones under traction or compression and the resulting stresses acting on the vessel wall. The results showed that the maximum structural stresses were located near the thin cap, a condition favorable for plaque rupture.

Acknowledgements

The authors acknowledge financial support from the Australian Research Council, under grant no. DP110100434.

References

[1] Avgerinos, E.D., Giannakopoulos, T.G., Kadoglou, N.P., et al. and Papapetrou, A., Biomarkers for Diagnosis of the Vulnerable Atherosclerotic Plaque, *Interventional Cardiology*, **3**(2), 2011, 223.

[2] Chaichana, T., Sun, Z. and Jewkes, J., Computational Fluid Dynamics Analysis of the Effect of Plaques on the Left Coronary Artery, *Comput. Math. Method M.*, **2012**, 2012, 1–9.

[3] Chatzizisis, Y.S., Coskun, A.U., Jonas, M., et al. and Stone, P.H., Role of Endothelial Shear Stress in the Natural History of Coronary Atherosclerosis and Vascular Remodelling: Molecular, Cellular and Vascular Behaviour, *J. Am. Coll. Cardiol.*, **49**(25), 2007, 2379–2393.

[4] Feintuch, A., Ruengsakulrach, P., Lin, A., et al. and Ethier, C.R., Hemodynamics in the Mouse Aortic Arch as Assessed by MRI, Ultrasound, and Numerical Modeling,*Am. J. Physiol. Heart Circ. Physiol.*, **292**, 2007, H884–H892.

[5] Feldman, C.L., Chatzizisis, Y.S., Coskun, et al. and Stone, P.H.,Vulnerable Anatomy; The Role of Coronary Anatomy and Endothelial Shear Stress in the Progression and Vulnerability of Coronary Artery Lesions: Is Anatomy Destiny?, *Contemp. Card.*, **5**, 2010, 495–506.

[6] Groen, H.C., Gijsen, F.J.H., Van der Lugt, A., et al. and Wentzel, J.J., Plaque Rupture in the Carotid Artery is Localized at the High Shear Stress Region,*Stroke*, **38**, 2007, 2379–2381.

[7] Han H.C, A biomechanical model of artery buckling,*J. Biomech.*, **40**(16), 2007, 3672–3678.

[8] Hannema, G.,*Three-dimensional fluid structure interaction methods applied to blood flow in straight vessels with atherosclerotic plaques.*, Master Thesis, Monash University, Clayton, Australia.

[9] Kock, S.A., Nygaard, J.V., Eldrup, N., et al. and Kim, W.Y., Mechanical Stresses in Carotid Plaques Using MRI-based Fluid-Structure Interaction Models,*J. Biomech.*, **41**, 2008, 1651–1658.

[10] Liu, Q. and Han H.C, Mechanical buckling of artery under pulsatile pressure,*J. Biomech.*, **45**, 2012, 1192–1198.

[11] Paidoussis, M. P., *Fluid-Structure Interaction, Slender Structures and Axial Flow*, Vol 1, Academic Press, 1998.

[12] Pello, O.M., Silvestre, C., Pizzol, M.D. and Andres, V., A Glimpse of the Phenomenon of Macrophage Polarisation During Atherosclerosis,*Immunobiology*, **216**, 2011, 1172–1176.

[13] Sadat, U., Teng, Z. and Gillard J.H., Biomechanical Structural Stresses of Atherosclerotic plaques,*Expert Review of Cardiovascular Therapy*, **8**(10), 2010, 1469–1481.

[14] Shinohara, M., Yamashita, T., Tawa, H., et al. and Momose, A.,Atherosclerotic plaque imaging using phase-contrast X-ray computed tomography, *Am. J. Physiol. Heart Circ. Physiol.*, **294**, 2008, H1094–H1100.

[15] Stone, P.H., Coskun, A.U., Kinlay, S., et al. and Feldman, C.L., Regions of Low Endothelial Shear Stress are the Sites where Coronary Plaque Progresses and Vascular Remodelling Occurs in Humans: an *in Vivo* Serial Study,*Eur. Heart J.*, **28**, 2007, 705–710.

[16] Tang, D., Teng, Z., Canton, G., Yang, C., et al. and Yuan, C., Sites of Rupture in Human Atherosclerotic Carotid Plaques are Associated with High Structural Stresses: An In Vivo MRI-Based 3D Fluid-Structure Interaction Study,*Stroke*, **40**, 2009, 3258–3263.

[17] Timoshenko, S.P. and Gere J.M., *Theory of Elastic Stability*, McGraw-Hill Book Company, Second edition, 1961.

[18] Trachet, B., Bols, J., De Santis, G., Vandenberghe, S., et al. and Segers, P., The Impact of Simplified Boundary Conditions and Aortic Arch Inclusion on CFD Simulations in the Mouse Aorta: A Comparison with Mouse-Specific Reference Data,*J. Biomech. Eng.*, **133**, 2011, 1–13.

[19] Vengrenyuk, Y., Kaplan, T.J., Cardoso, L., et al. and Weinbaum, S., Computational Stress Analysis of Atherosclerotic Plaques in ApoE Knockout Mice, *Ann. Biomed. Eng.*, **38**(3), 2010, 738–747.

[20] Wells, R.E., Merrill J.W. and Merrill, E.W, Shear rate dependence of the viscosity of whole blood and plasma, *science*, **133**(3455), 1961, 763–764.

[21] Young, F.D. and Tsai F.Y., Effect of a time dependent stenosis on flow through a tube, *Journal of Engineering for Industry-Transactions of the ASME*,**90**, 1968, 248–254.